Probing Microstructure Evolution during the Hardening of Gypsum by Proton NMR Relaxometry

Hamouda Jaffel,[†,‡] Jean-Pierre Korb,*[,†] Jean-Philippe Ndobo-Epoy,[‡] Vincent Morin,[‡] and Jean-Pierre Guicquero[‡]

Laboratoire de Physique de la Matière Condensée, UMR 7643 du CNRS, École Polytechnique, 91128 Palaiseau Cedex, France, and Lafarge, Centre de Recherche, 38291 Saint-Quentin Fallavier Cedex, France

Received: October 21, 2005; In Final Form: February 2, 2006

We report a comprehensive proton NMR relaxation study of the water confined in the evolving porous structure of hardened gypsum prepared with different water-to-plaster ratios (w/p) and increasing additions of crushed gypsum. This study gives some new information on the microstructure, the water distribution, and the hydration kinetics without any drying or perturbing preparation. The bi-exponential transverse magnetization decay reveals the existence of two water populations in slow exchange. However, the different behaviors of these populations during saturation and desaturation experiments show evidence of a fast exchange of each population with the surface. Two modes of organization of the microstructure of this material are identified through an original model of exchange as a function of the water-to-plaster ratio ($0.4 \leq w/p \leq 0.6$ and $0.7 \leq w/p \leq 1$). A clear gap is shown in the exchange rate value above $w/p = 0.6$ that could be representative of a percolation threshold. Both the method and the theory presented can be applied more widely to other porous media with reactive surface areas.

I. Introduction

How does the microstructure of a reactive porous medium appear and evolve during the hydration and setting, and how is it possible to follow these processes by nondestructive techniques? Here, we propose to answer this question in the case of gypsum, a material of general interest in civil engineering. Basically, there are two main objectives in the research on gypsum: (i) to improve the knowledge of the main steps of hydration of plaster to give key parameters for the mixing efficiency of this material; (ii) to improve the mechanical properties by a better knowledge of the microstructure (specific surface area, pore size distribution and connectivity) in this disordered solid system.

It is well known that proton NMR spectroscopy evidences the proton chemical species within the gypsum crystal.[1] It is also well known that proton NMR relaxometry of mixing water is well adapted to probe continuously the evolution of cement paste without perturbing the system.[2−7] With NMR techniques, no drying is necessary that could produce nanostructure modifications, by nonwetting fluid intrusion (nitrogen adsorption or mercury intrusion porosimetry). However, to our knowledge, there is no comprehensive proton NMR relaxometry study allowing a direct nonperturbative characterization of the evolving microstructure of this building material.

Here, we propose such a proton relaxometry at low magnetic fields during the setting of plaster. First, we studied the NMR transverse relaxation of water confined in the porous media of hardened gypsum prepared with several water-to-plaster ratios (w/p) between 0.4 and 1 and with an increasing addition of crushed gypsum. Second, we used the water fraction values obtained by a bi-exponential fit of the measured transverse relaxation decay, to follow the hydration kinetics and to provide some details of the evolving porous structure during the setting of plaster pastes prepared with several formulation parameters. We show that there are two evolution modes of organization of the microstructure in the range ($0.4 \leq w/p \leq 0.6$) and ($0.7 \leq w/p \leq 1$) in agreement with pulsed field gradient experiments.[8−10] Then, we developed saturation *(water re-impregnation)* and desaturation *(drying)* experiments in order to obtain some information about water dynamics in pores of hardened gypsum. Finally, we proposed a detailed original model explaining the slow exchange mode that can exist between water populations saturating the material. The typical variation observed for the rate of exchange with the water-to-plaster ratio confirms the presence of two evolution modes of organization in the materials. We believe that our experimental method (proton NMR relaxometry at low magnetic field) is fast and robust enough to follow the progressive setting of the reactive interface of other building materials or, more generally, to follow that of any porous medium without any dehydration.

II. Materials and Methods

Calcium sulfate hemihydrate ($CaSO_4 \cdot {}^1/_2H_2O$), usually called plaster, comes from the dehydration of calcium sulfate dihydrate ($CaSO_4 \cdot 2H_2O$), usually called gypsum. There are two varieties of plaster, α and β, produced by wet or dry methods, respectively.

The hydration of plaster can be described in the following way.[11,12] In the first step, the dissolution of hemihydrate leads to calcium and sulfate ions. The crystallization of gypsum starts as soon as oversaturation is reached. Then, two chemical

* Corresponding author. E-mail address: jean-pierre.korb@polytechnique.fr.
† Laboratoire de Physique de la Matière Condensée.
‡ Lafarge, Centre de Recherche.

10.1021/jp058276m CCC: $33.50
Published on Web 03/11/2006

reactions occur simultaneously:

$$CaSO_4 \cdot {}^1/_2H_2O_{(solid)} \rightarrow Ca^{2+}{}_{(aq)} + SO_4{}^{2-}{}_{(aq)} + {}^1/_2H_2O_{(aq)}$$

$$Ca^{2+}{}_{(aq)} + SO_4{}^{2-}{}_{(aq)} + 2H_2O_{(aq)} \rightarrow CaSO_4 \cdot 2H_2O_{(solid)}$$

These two equations thus give the following:

$$CaSO_4 \cdot {}^1/_2H_2O_{(solid)} + {}^3/_2H_2O_{(aq)} \rightarrow CaSO_4 \cdot 2H_2O_{(solid)}$$

We used a commercial β-plaster (Meriel quarry, Lafarge Plaster, France) with a purity of 96 wt %. According to these reactions, the stoichiometric water-to-plaster weight ratio is 0.186. The ratio generally used in gypsum industry lies between 0.4 and 1, i.e. much higher than 0.186. Such an excess of water enables the development of porosity. The hardening of a plaster paste leads to a permeable porous structure, made of entangled needle-shape gypsum crystals.

The samples were prepared by manual mixing of plaster powder and distilled water, at well-defined water-to-plaster weight ratios (w/p) from 0.4 to 1. In some experiments, some crushed gypsum was added to change the hydration kinetics and the microstructure configuration. The plaster paste was weighted and introduced into a sealed NMR tube, to avoid evaporation during the experiment. The time acquisition was started at the beginning of the mixing of plaster and water. The NMR acquisition was started a few minutes later. The temperature regulation of the NMR apparatus was set to 25 °C.

^{1}H (NMR) relaxometry experiments were performed using a low field spectrometer Maran-Ultra (0.55 T) from Oxford Instruments Molecular Biotools (England), operating at the proton Larmor frequency of 23 MHz. The transverse relaxation decays were measured by the well-known Carr−Purcell−Meiboom−Gill (CPMG) sequence, used to avoid the phase shifts due to local inhomogeneities of the magnetic field.[13] This CPMG sequence was performed during the whole hydration process of plaster in order to study the kinetics of the hydration reaction. The inter-echo delay was 800 μs, and the duration of a whole sequence was about 0.8 s. For the kinetics study, each sequence has been accumulated four times and was repeated every minute during 1 h. For the studies on hardened gypsum, the NMR sequences have been realized after a time scale of 1 or 2 h that is much larger than the setting time (about 30 min). With this spectrometer, the solid protons within the gypsum crystals and those belonging to chemically bound water cannot be detected, since their relaxation times are far too short.[2,4,6] Consequently, their relaxation components could not contribute to the echo signals in our experiments. Thus, the total intensities of the NMR signals were proportional to the amount of mobile water molecules.

Complementary standard experiments were performed to characterize the porous structure of hardened gypsum. Before the experiments, the samples were dried at 45 °C overnight. Nitrogen adsorption was used on a Beckman Coulter SA3100 to measure the Brunauer−Emmett−Teller (BET) specific surface area.[14] We measured the porosity of these samples by mercury intrusion with a Micromeritics Auto poreIII. We used field effect scanning electron microscopy (SEM) JEOL 5800LV under high vacuum and metallization to obtain images of our samples.

III. Results and Discussion

A. Relaxation of Water in Hardened Gypsum. The first result is the relaxation curve obtained by the CPMG sequence and presented in Figure 1. This figure shows a typical normalized transverse proton magnetization decay $M_{xy}(t)/M_0$ (over two decades) of water filled hardened gypsum obtained after 2 h of hydration ($w/p = 0.8$). We repeated the experiment varying the echo time spacings ($= 2\tau$ where τ is the 90−180° pulse gap in the CPMG sequence) between 0.4 and 4 ms and noticed no modification in the transverse relaxation data that can reveal some gradient field inhomogeneity effects. This proves that, at this low frequency (23 MHz), there is no inhomogeneity of susceptibility.[1] The dashed line represents the best least-squares fit obtained with a bi-exponential decay function $F(t)$ with an offset correction.

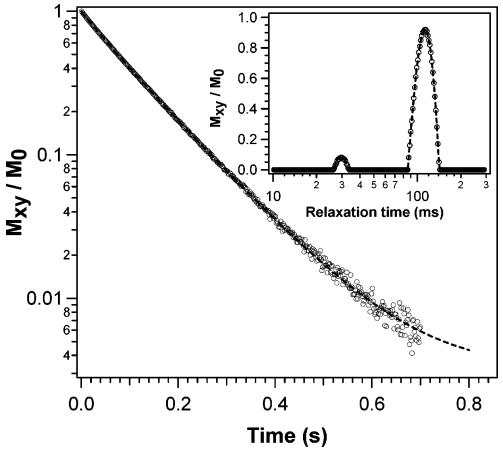

Figure 1. NMR transverse relaxation decay (CPMG sequence) from the water confined in the porous medium of hardened gypsum, (water-to-plaster ratio (w/p) of 0.8). The dashed line represents a fit with a double-exponential function, indicating that there are two proton populations. There is a good correlation with the results of the inverse Laplace transform of the relaxation decay (inset), showing two protons populations.

$$F(t) = a \exp(-R_{2,slow}t) + b \exp(-R_{2,fast}t) + c \qquad (1)$$

where t is the time and $R_{2,fast}$ and $R_{2,slow}$ are the corresponding transverse rate constants associated with the two magnetization fractions (or proton populations) a and b ($a + b \approx 1$). The offset c was used to take into account the very small asymptotic normalized magnetization typically about 10^{-3} (signal-to-noise ratio about *500*). For all the fits, the data were restricted to values such that $F(t) = M_{xy}(t)/M_0 \geq 0.01$. We have displayed in the inset of Figure 1 the inverse Laplace transform of the normalized magnetization decay performed with the WinDXP software (Oxford Instruments) that confirms the existence of these two proton populations. We tried to fit the signal with a sum of 3 or 4 exponentials and checked that their contributions were much lower than a few percent of the total signal. The same observation was made for all the magnetization decays presented in this paper. Consequently, we have assumed that all these magnetization decays were accurately fitted by two-exponential functions.

From a physical point of view, we obtain two kinds of information. (i) The transverse relaxation rate constants (R_2) can be associated with the dynamics of mobile water molecules.[1] (ii) The magnetization fraction provides a quantitative measurement of water in both populations. In Figure 1 where $w/p = 0.8$, the first component has the higher proton population ($a \sim 90\%$) and the smaller relaxation rate $R_{2,slow} = 8.3\ s^{-1}$ ($T_{2,long} = 1/R_{2,slow} = 121$ ms). The second component has the lower proton population ($b \sim 10\%$) and the larger relaxation rate $R_{2,fast} = 20.3\ s^{-1}$ ($T_{2,short} = 1/R_{2,fast} = 49$ ms). On the other hand, the

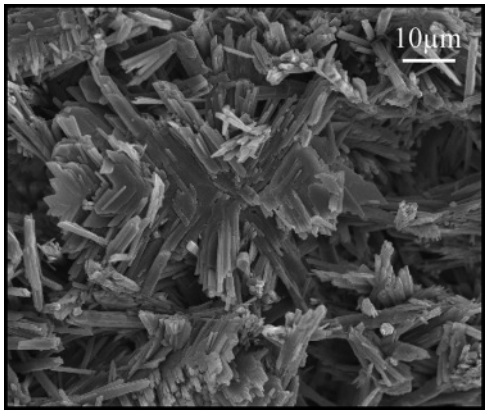

Figure 2. SEM photomicrograph showing a typical view of the microstructure of hardened gypsum, prepared with a water-to-plaster ratio of 0.8. The length scale bar is 10 μm.

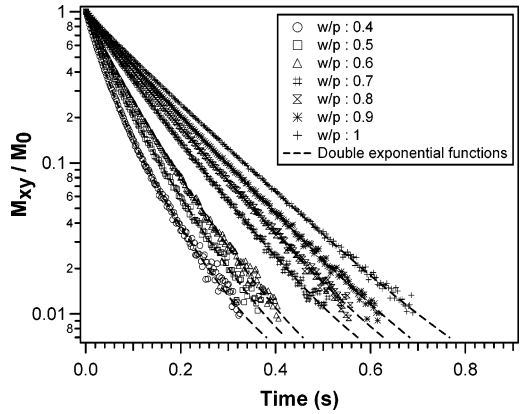

Figure 3. Transverse relaxation decays (measured by the CPMG sequence) of water confined in the porous medium of hardened gypsum, prepared with different water-to-plaster ratios (1, 0.9, 0.8, 0.7, 0.6, 0.5, and 0.4), plotted as a function of time. The dashed lines are sums of two exponential functions, fitting the experimental signals with a good accuracy.

TABLE 1: Results of the Double-Exponential Functions Fitting the Transverse Relaxation Decays of Figure 3, with Various Water-to-Plaster Ratios[a]

$F(t) = a \exp[-tR_{2,\text{slow}}] + b \exp[-tR_{2,\text{fast}}] + c$

w/p	1	0.9	0.8	0.7	0.6	0.5	0.4
a	0.93	0.91	0.87	0.82	0.66	0.55	0.41
$R_{2,\text{slow}}$ (s^{-1})	6.8	7.5	8.3	9.1	10.9	11.4	12.5
b	0.07	0.09	0.13	0.18	0.34	0.45	0.59
$R_{2,\text{fast}}$ (s^{-1})	19.7	20.5	20.3	21.8	24.0	26.7	33.2

[a] The terms a and b are the volume fractions of the proton populations, much higher than the offset constant $c \approx 10^{-3}$.

hardening of plaster paste leads to a permeable porous structure, made of entangled needle-shape gypsum crystals, observed in Figure 2. In regards to the spatial localization of these two water populations, a hypothesis might be that the first population (associated with the longer T_2) extends uniformly in space while the second water population (with the shorter T_2) is more confined and isolated in some clusters of gypsum needles. We aim, in the following, at addressing this hypothesis.

To understand the origin of this distribution of proton populations, we made several proton relaxometry measurements (Figure 3) at different w/p ratios (w/p: 1, 0.9, 0.8, 0.7, 0.6, 0.5, 0.4). We succeeded in fitting the data of Figure 3 with eq 1 and reported in Table 1 the obtained values of a, b, $R_{2,\text{slow}}$, and $R_{2,\text{fast}}$. We observed that the magnetization decay is all the faster (increase of $R_{2,\text{fast}}$ and $R_{2,\text{slow}}$) as w/p decreases. An inversion

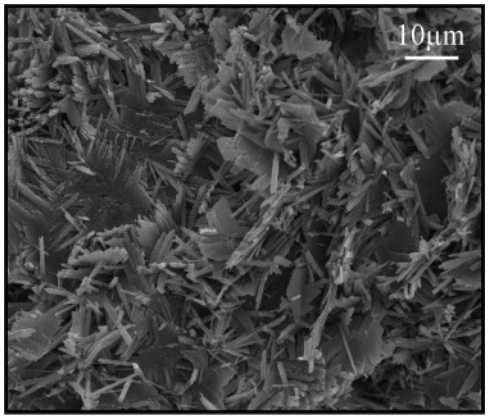

Figure 4. SEM photomicrograph showing a typical view of the microstructure of hardened gypsum, prepared with a water-to-plaster ratio of 0.8 and 0.04 wt % of crushed gypsum. The length scale bar is 10 μm.

TABLE 2: Porosity of the Hardened Gypsum Measured by Mercury Intrusion as a Function of the Water-to-Plaster Ratio w/p

w/p	0.4	0.5	0.6	0.7	0.8	0.9	1
porosity (%)	36	44	51	55	58	60	61

of the values of a and b was observed between $w/p = 0.5$ and 0.4. We also measured the porosity of these samples of hardened gypsum by mercury intrusion porosimetry (MIP). As seen in Table 2, the higher the w/p ratio, the higher the porosity. Both results (MIP and NMR) are thus consistent: the lower the porosity, the lower the mobility of water and the faster the relaxation.

We noted a clear gap between the magnetization decays corresponding to $0.7 \leq w/p \leq 1$ and those corresponding to $0.4 \leq w/p \leq 0.6$ (Figure 3). We assumed at this stage that this gap was the signature of an important modification in the organization of the porous structure of hardened gypsum. Similar phenomena were observed by Filippov et al.[8] with NMR pulsed field gradient measurements of self-diffusion of liquids confined in the pores of gypsum and were interpreted in terms of a model with two levels of organization of the porous structure.

In other experiments, we measured the transverse relaxation decays M_{xy}/M_0 of samples having the same water-to-plaster ratio $w/p = 0.8$ but increasing amounts of crushed gypsum (CG, 0 (reference), 0.004, 0.04, 0.1, 0.5 wt %). This modifier is known for its high acceleration efficiency of the hydration process[15] and its ability to change the shape of the gypsum crystals (Figure 4) and, hence, the total specific surface area. The magnetization decays M_{xy}/M_0 of these samples are displayed in Figure 5. It is clear that these plots exhibit a non-monoexponential behavior, indicating at least double-exponential components. The results of double-exponential fits are reported in Table 3. An inversion of the water populations when increasing the amount of crushed gypsum (from 0.1% CG) is observed, similar to the previous experiments with various w/p values. The magnetization decays presented in Figure 5 and the values of Table 3 clearly illustrate the effects of the crushed gypsum on the spatial distribution of water: the higher the amount of crushed gypsum, the higher the relaxation rate, thus the lower the mobility of water. We also measured the specific surface area of these samples by nitrogen adsorption (Table 4). We observe that the higher the amount of crushed gypsum, the higher the specific surface area.

Contrarily to the previous experiments with decreasing w/p, where we observed an important decrease of the porosity, we

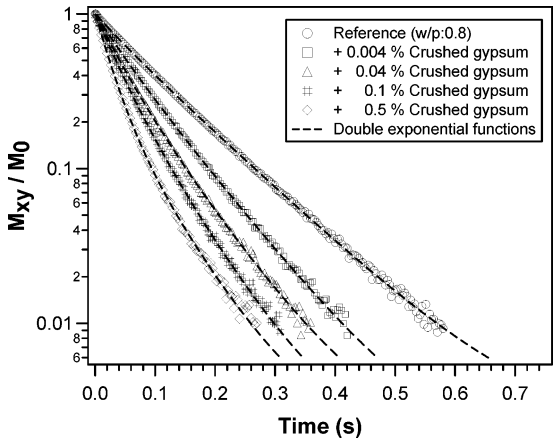

Figure 5. Transverse relaxation decays (measured by the CPMG sequence) of the water confined in the porous medium of hardened gypsum plotted as a function of time. The samples were prepared with a *w*/*p* of 0.8 and with various additions of crushed gypsum. The dashed lines represent the double-exponential functions fitting the signals.

TABLE 3: Results of the Double-Exponential Fits of the Transverse Relaxation Decays of Set Plaster Prepared with an Increasing Percentage of Crushed Gypsum[a]

$F(t) = a \exp[-tR_{2,\text{slow}}] + b \exp[-tR_{2,\text{fast}}] + c$

CG *(%)*	0 ref	0.004	0.04	0.1	0.2	0.5
a	0.87	0.75	0.54	0.46	0.37	0.31
$R_{2,\text{slow}}$ (s^{-1})	8.3	10.9	12.0	13.6	13.1	13.9
b	0.13	0.25	0.46	0.54	0.63	0.69
$R_{2,\text{fast}}$ (s^{-1})	20.3	22.8	24.6	27.8	29.9	38.5

[a] The terms *a* and *b* are the volume fractions of the proton populations, much higher than the offset constant $c \approx 10^{-3}$.

TABLE 4: Specific Surfaces Measured by the Nitrogen Adsorption Technique (BET-N_2)[a]

CG (wt %)	0	0.004	0.02	0.04	0.1	0.2	0.5
Sp-N_2 (m^2/g)	0.95	1.1	1.2	1.4	1.6	1.66	1.73

[a] The samples were prepared with a *w*/*p* of 0.8 and with various additions of crushed gypsum.

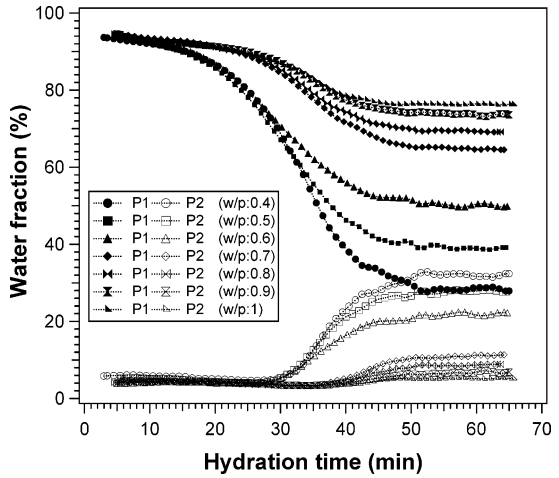

Figure 6. Evolution of the two water populations (P_1 and P_2) in plaster pastes prepared with various *w*/*p* (1, 0.9, 0.8, 0.7, 0.6, 0.5, and 0.4) as a function of the hydration time. The signals were normalized by the total magnetization at mixing $M(t = 0)$.

could not determine any difference in the porosities of the samples (~58%) prepared with several additions of crushed gypsum.

B. Kinetics of Hydration. In Figure 6, we have displayed the evolution of the two water populations (at different *w*/*p* ratios, without crushed gypsum) as a function of hydration time during the setting of plaster. It took about 1 h to complete the hydration process. In this case, we have to take into account the consumption of water by the hydration reaction to form the solid gypsum crystal. So, we have to introduce new variables (P_1 and P_2) instead of previously defined *a* and *b* to follow the amount of the water population that progressively evolved in time. For the sake of simplicity, we have normalized these populations to the initial total magnetization ($P_1 + P_2 = M_{xy}(t_{\text{hydration}})/M_{xy}(t_{\text{hydration}} = 0)$. The water consumption necessary for the hydration reaction as a function of time can thus be quantitatively followed. We observe that the lower the *w*/*p* ratio, the higher the consumption of water. The water population P_1 was always decreasing as a function of time, whatever the *w*/*p* ratio. On the other hand, the second water population P_2 was always increasing as a function of hydration time. Simultaneously, we note that the lower the *w*/*p* ratio, the lower the P_1 population and the higher the P_2 population. Once again, we observe a considerable variation between the evolution of the water distribution corresponding to $0.7 \leq w/p \leq 1$ and those corresponding to $0.4 \leq w/p \leq 0.6$. This result can be associated to a threshold ratio (*w*/*p*) from which the microstructural organization changes a lot. We did the same experiment with the previous amounts of crushed gypsum. On Figure 7, we clearly see the high acceleration efficiency of crushed gypsum on the hydration of plaster. The proportion of water corresponding to the second population P_2 increased with the crushed gypsum amount. Moreover, the crossing over of the two populations was all the clearer since the initial amount of crushed gypsum was high enough. We note that the variation of the *w*/*p* and the addition of crushed gypsum lead to samples with almost similar distributions of water populations but having different microstructures (e.g., $w/p = 0.8$ without CG, Figure 6, and $w/p = 0.8$ with 0.04% CG, Figure 7). Consequently, the water distribution measured by NMR relaxometry cannot be directly correlated to a unique well-defined microstructure.

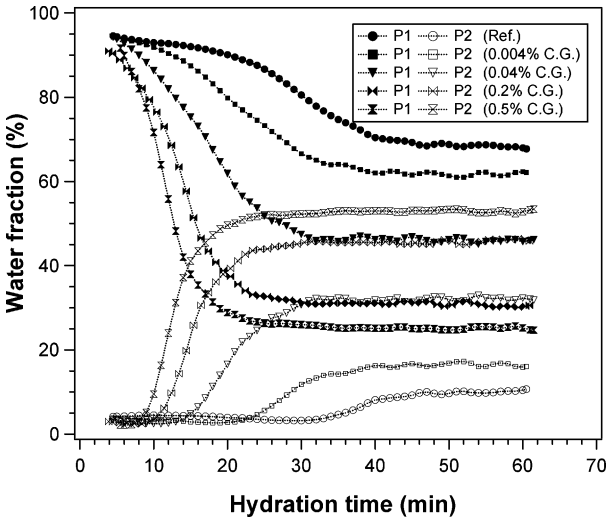

Figure 7. Evolution of the two water populations (P_1 and P_2) in plaster pastes as a function of hydration time, prepared with a *w*/*p* of 0.8 and with various additions of crushed gypsum (CG). The signals were normalized by the total magnetization at mixing $M(t = 0)$.

C. Regime of Water Relaxation in Hardened Gypsum. What is the limiting factor of relaxation of water in hardened gypsum? Brownstein and Tarr,[16] Kleinberg,[17] and Godefroy[18] gave an extensive description of the relaxation of water in porous media. These authors have shown that the relaxation decay in simple pore geometries is dominated by the value of the

dimensionless parameter $\rho_2 r/2D$, where ρ_2 is the surface relaxivity, D is the self-diffusion coefficient ($D = 2.3 \times 10^{-9}$ $m^2 \cdot s^{-1}$ for water at room temperature), and r is the typical pore size. Two limiting cases exist: (i) $\rho_2 r/2D \gg 1$ corresponds to the slow diffusion limit. Here, the relaxation is limited by the surface access time. This is the case of large pores and/or high surface relaxivities. (ii) $\rho_2 r/2D \ll 1$ corresponds to the fast diffusion limit. In this regime, the relaxation is limited by the surface relaxation. Introducing V as the varying volume of water, S as the surface of the pore, and V_0 as the maximum volume reached, the transverse relaxation time can be written (according to the biphasic fast exchange model[19−21]) as

$$(T_2)_{meas} \approx [V_0/(S\rho_2)](V/V_0) \quad (2)$$

This equation clearly exhibits the linearity of the measured relaxation time as a function of the filling factor V/V_0.

To characterize the dynamical process at the origin of the proton relaxation in pores of hardened gypsum, we have followed the evolution of the normalized total magnetization $P_1 + P_2 = M_{xy}(V/V_0)/M_{xy}(V/V_0 = 1)$, as well as transverse relaxation times and populations P_1 and P_2 by varying the filling factor V/V_0. The transverse relaxation time previously described ($T_{2,long}$ or $T_{2,short}$) was measured during the two following experiments: (i) The first experiment was a progressive drying of the sample at 45 °C and 20% RH, starting with a fully saturated sample. (ii) The second experiment was a progressive re-impregnation or saturation experiment with increasing volumes of a saturated solution of calcium sulfate (in order to limit the dissolution of gypsum that could produce some structural modifications). The sample was initially dried for 24 h at 45 °C. The temperature of 45 °C was chosen to enable the evaporation of water in the pores without inducing any dehydratation of gypsum, and the saturation experiment is carried out by solution pumping inside the porous media.

The relaxation times $T_{2,long}$ and $T_{2,short}$ and their associated water fractions P_1 and P_2 during saturation and desaturation experiments are respectively reported in Figures 8 and 9. These figures lead to the following conclusions: (i) We observe linear dependences of the transverse relaxation time $T_{2,long}$ (Figure 8) and of P_1 (Figure 9) with V/V_0 for both saturation and desaturation experiments. As shown by Halperin et al.,[19−21] these observations are characteristic of a fast diffusion relaxation process between the surface and bulk water. We also see a slight difference between the saturation slope and the desaturation one (Figure 8a). This is explained by the crystallization of gypsum needles, since the solution is oversaturated during the drying of the sample. (ii) On the other hand, the evolutions of the relaxation time $T_{2,short}$ (Figure 8a) and of P_2 (Figure 9) with V/V_0, during the saturation and the desaturation experiment, exhibit a clear hysteresis. This result strongly suggests a higher porous confinement of this water population that supports the development of water menisci during these two experiments. We also note that, after a given plateau, the evolution of the relaxation time $T_{2,short}$ becomes a linear function of V/V_0 in the range $0.1 \leq V/V_0 \leq 0.7$ for the desaturation and in the range $0.7 \leq V/V_0 \leq 1$ for the saturation, which implies a fast diffusion process too. Moreover, the desaturation experiment exhibits a well-defined relaxation time plateau for $0.02 \leq V/V_0 \leq 0.04$ (Figure 8b) that gives a measurement of the surface relaxation time $T_{2,surf} \sim 200$ μs. We confirm this value by decreasing the interecho time spacing to 60 μs in a dry sample.

According to this measured value of the surface relaxation time and assuming a water layer width $\lambda \sim 1$ nm (about three monolayers, according to previous calorimetric and NMR studies

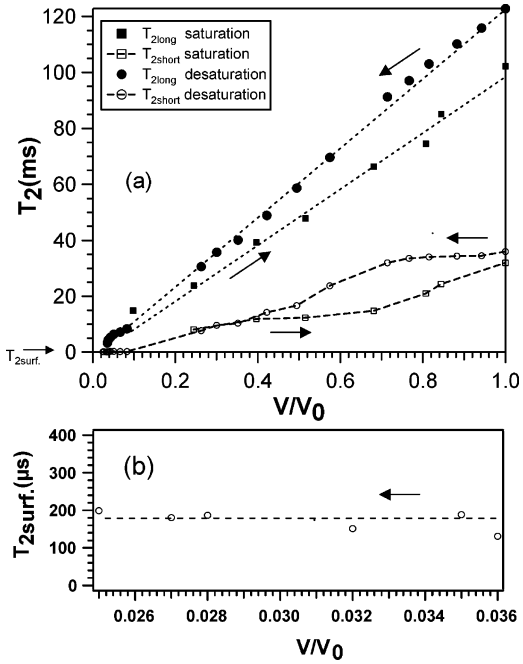

Figure 8. (a) Transverse relaxation times $T_{2,long}$ and $T_{2,short}$ associated with the proton populations P_1 and P_2 plotted as a function of water contents (V/V_0) during filling (■ P_1, □ P_2) and drying (● P_1, ○ P_2) experiments on a sample of hardened gypsum ($w/p = 0.8$). (b) Surface layer relaxation time (obtained by a zoom of the desaturation plateau of part a).

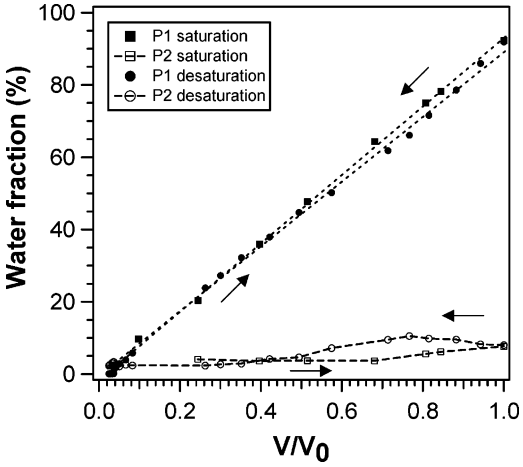

Figure 9. Evolution of the water fractions corresponding to populations P_1 and P_2 during filling and drying experiments on a sample of hardened gypsum ($w/p = 0.8$).

developed by Fripiat et al.[22]), the value of the surface relaxivity $\rho_2 = \lambda/T_{2,surf}$ can be estimated at about 5 $\mu m \cdot s^{-1}$. Assuming a cylindrical pore size of approximately 5 μm (estimated by MIP) for hardened gypsum, one finds $\rho_2 r/2D = 0.0054 \ll 1$, thus justifying the fast diffusion regime. The relaxation process is thus limited by the solid−liquid interaction at the interface and not by the transport of water molecules to the surface.

D. Model of Exchange between Two Proton Populations. To explain the coexistence of two different water populations, both following the fast diffusion model, we detail the relaxation process in the porosity of hardened gypsum. In reality, these water populations are interconnected, and within the time scale of an NMR experiment, the liquid molecules may diffuse in the interconnected pore structure before a significant part of the magnetization relaxes.

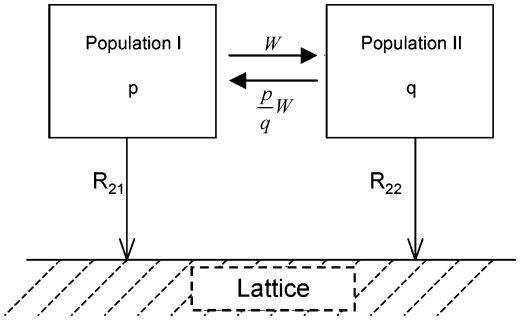

Figure 10. Schematic model describing the exchange rate W between the proton populations P_1 and P_2 having the relaxation rates, R_{21} and R_{22}, and associated with the weight factors p and q, respectively.

We determine their exchange rate by the following model (Figure 10). We consider that the transverse relaxations of the two water populations of magnetizations, $M_{+1}(t)$ and $M_{+2}(t)$, are coupled by a more or less efficient exchange process characterized by an exchange rate W. The individual weight factors are p and q (with $p + q = 1$), and the relaxation rates are R_{21} and R_{22}. From Figure 10, we can write the following coupled Bloch equations:

$$\frac{\mathrm{d}}{\mathrm{d}t}\begin{bmatrix}M_{+1}(t)\\M_{+2}(t)\end{bmatrix} = \begin{bmatrix}-(R_{21}+W) & W\frac{p}{q}\\ W & -\left(R_{22}+W\frac{p}{q}\right)\end{bmatrix}\begin{bmatrix}M_{+1}(t)\\M_{+2}(t)\end{bmatrix} \quad (3)$$

The solution of these coupled differential equations is a linear combination of two exponentials whose rate constants, $R_{2,\mathrm{slow}}$ and $R_{2,\mathrm{fast}}$, are the eigenvalues of matrix 3. In practice, we measured the overall magnetization $M_+(t) = M_{+1}(t) + M_{+2}(t)$, given by the following expression:

$$M_{\mathrm{norm}}(t) = \frac{M_+(t)}{M_+(0)} = \frac{1}{2\sqrt{\Delta}}\left\{\left[p\left(-R_{21}+R_{22}+\frac{W}{q}+\sqrt{\Delta}\right)+q\left(R_{21}-R_{22}+\frac{W}{q}+\sqrt{\Delta}\right)\right]\exp(-R_{2,\mathrm{slow}}t)+\left[p\left(R_{21}-R_{22}-\frac{W}{q}+\sqrt{\Delta}\right)+q\left(-R_{21}+R_{22}-\frac{W}{q}+\sqrt{\Delta}\right)\right]\exp(-R_{2,\mathrm{fast}}t)\right\}+c = a\exp(-R_{2,\mathrm{slow}}t)+b\exp(-R_{2,\mathrm{fast}}t)+c \quad (4)$$

where

$$R_{2,\mathrm{slow}} = \frac{1}{2}\left(R_{21}+R_{22}+\frac{W}{q}-\sqrt{\Delta}\right)$$

$$R_{2,\mathrm{fast}} = \frac{1}{2}\left(R_{21}+R_{22}+\frac{W}{q}+\sqrt{\Delta}\right)$$

$$\sqrt{\Delta} = \sqrt{(R_{21}-R_{22})^2+\left(\frac{W}{q}\right)^2+2W\left(1-\frac{p}{q}\right)(R_{21}-R_{22})} \quad (5)$$

When $W = 0$ (i.e., in the absence of exchange), one can verify that eq 4 tends to eq 1, where ($p = a$, $q = b$) and ($R_{2,\mathrm{slow}} = R_{21}$, $R_{2,\mathrm{fast}} = R_{22}$). To simplify the previous equations, we consider the following two limiting cases.

(i) In the case of fast exchange, $W \gg R_{21}$; R_{22}; $|R_{21} - R_{22}|$ with $R_{22} > R_{21}$, and eqs 5 become:

$$R_{2,\mathrm{slow}} \approx pR_{21} + qR_{22}$$

$$R_{2,\mathrm{fast}} \approx qR_{21} + pR_{22} + \frac{W}{q} \approx \frac{W}{q}$$

$$\sqrt{\Delta} = \frac{W}{q} + (q-p)(R_{21}-R_{22}) \approx \frac{W}{q} \quad (6)$$

$$M_{\mathrm{norm}}(t) \approx \frac{2W}{q}\exp(-R_{2,\mathrm{slow}}t) + c \quad (7)$$

i.e., a monoexponential time decay.

(ii) In the case of a slow exchange, $W \ll R_{21}$ or R_{22} and $W \ll |R_{21} - R_{22}|$ with $R_{22} > R_{21}$, and eqs 5 become:

$$R_{2,\mathrm{slow}} \approx R_{21} + W$$

$$R_{2,\mathrm{fast}} \approx R_{22} + \frac{p}{q}W$$

$$\sqrt{\Delta} = R_{22} - R_{21} + \frac{W}{q}(p-q) \quad (8)$$

$$M_{\mathrm{norm}}(t) \approx p\left(1+\frac{2W}{R_{22}-R_{21}}\right)\exp(-R_{2,\mathrm{slow}}t) + q\left(1-\frac{2(p/q)W}{R_{22}-R_{21}}\right)\exp(-R_{2,\mathrm{fast}}t) + c \quad (9)$$

i.e., a sum of two exponentials time decays. We can thus deduce the corrected values of water fraction and relaxation rates as function of the exchange rate W:

$$p(W) = a\left(1-\frac{2W}{R_{2,\mathrm{fast}}-R_{2,\mathrm{slow}}}\right)$$

$$R_{21}(W) = R_{2,\mathrm{slow}} - W$$

$$R_{22}(W) = R_{2,\mathrm{fast}}\left(\frac{1-a+a\epsilon}{1-a+2a\epsilon}\right) \quad \text{with } \epsilon = \frac{W}{R_{2,\mathrm{fast}}-R_{2,\mathrm{slow}}} \quad (10)$$

To determine the exchange rate value W from our experimental data, we use the following procedure. First, we fit the experimental data of hardened gypsum with the sum of two exponentials to find ($R_{2,\mathrm{slow}}$, $R_{2,\mathrm{fast}}$) and (a, b). Then, we used these values to fit the signal with eqs 4, 5, and 10 describing the particular situation of a slow exchange. The results of the fits for different values of w/p are reported in Table 5. For instance, we have displayed, in Figure 11, a typical normalized magnetization decay of water filled hardened gypsum ($w/p = 0.8$) where we found an exchange rate value, $W \sim 0.2\ \mathrm{s}^{-1}$, much slower than the relaxation rates R_{21} and R_{22}.

In Figure 12a is displayed the variation of W with w/p that presents a step function behavior: $W \approx 0.2\theta[(w/p) - (w/p)_{\mathrm{threshold}}]$ with $(w/p)_{\mathrm{threshold}} \sim 0.6$. This behavior is a key result of this study that is indicative of a percolation threshold for water between two modes of organization of the microstructure

TABLE 5: Exchange Rate W Calculated Using Equations 4 and 5, Describing the General Situation, Water Fractions (p, q), and Their Associated Relaxation Rates (R_{21}, R_{22}) Calculated for Several Water-to-Plaster Rates (w/p) Using Equation 10

w/p	1	0.9	0.8	0.7	0.6	0.5	0.4
$W\ (\mathrm{s}^{-1})$	0.17	0.20	0.18	0.19	0.00	0.00	0.00
$p(W)$	0.91	0.88	0.84	0.80	0.66	0.55	0.41
$R_{21}\ (\mathrm{s}^{-1})$	6.63	7.30	8.12	8.91	10.90	11.40	12.50
$q(W)$	0.09	0.12	0.16	0.20	0.34	0.45	0.59
$R_{22}\ (\mathrm{s}^{-1})$	18.08	19.02	19.33	21.06	24.00	26.70	33.20

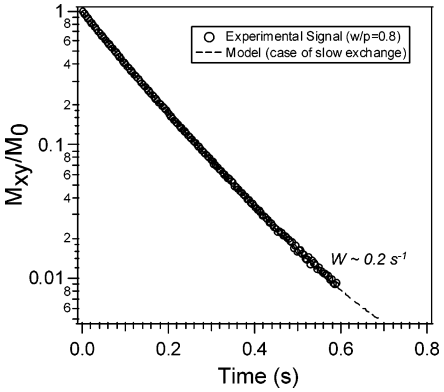

Figure 11. Transverse magnetization decay (measured using CPMG sequence) of water confined in a sample of hardened gypsum ($w/p = 0.8$) plotted as function of time. The dashed line represents a fit using eqs 4, 5, and 10 with an exchange rate $W_{fit} \sim 0.2\ s^{-1}$, much lower than R_{21} and R_{22}.

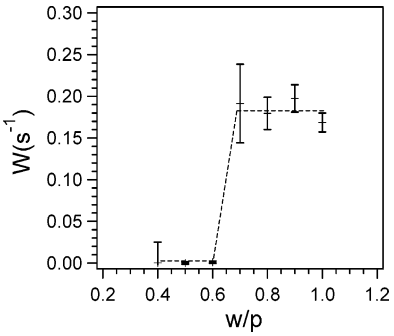

Figure 12. Exchange rate W (s^{-1}) associated with several water-to-plaster ratios, obtained by fitting the experimental signals with eqs 4, 5, and 10.

of this material. Below $w/p \leq 0.6$, one observes an extremely slow exchange rate (almost zero) and the two water populations are thus independent at least on the time scale of the experiment. Above $w/p \geq 0.7$, one observes a constant value $W \sim 0.2\ s^{-1}$ characteristic of a small but finite exchange rate between the two water populations.

We introduce now the diffusion length l_D necessary for exchanging (by isotropic diffusion) these two water populations on the time scale of $1/W$:

$$l_D = \sqrt{6D_{gypsum}/W} \tag{11}$$

where $D_{gypsum} \approx D_{bulk}/\tau$ is the approximated self-diffusion coefficient of water confined in pores of gypsum medium ($D = 2.3 \times 10^{-9}\ m^2 \cdot s^{-1}$ for bulk water at room temperature, and τ is the tortuosity factor in porous media). If we follow ref 23 that relates τ with the porosity ϕ for a given network, one has $\tau \sim 2$ for $\phi \sim 50\%$. Substituting this latter value into eq 11, we obtain a maximal length scale $l_D \sim 185\ \mu m$ (about 10 times the length of a single gypsum needle). The step variation behavior of $W(w/p)$ is also consistent with the NMR results shown in Figures 3 and 6. From a microstructural point of view, this result might reveal the presence of two intricated percolation networks of needles with different packing density where the percolation threshold for allowing the water exchange is about $w/p = 0.6$. The location of such a threshold is intrinsic to the water confinement within the particular packing of this polycrystalline material. The situation is very different for cement pastes where the multi-exponential behavior of the proton relaxation of such a multiphase disordered material revealed clearly different pore modes.[24,25]

IV. Conclusion

We have presented a comprehensive ^1H NMR relaxation study of water confined in the porous medium of hardening gypsum, during and after setting. The coexistence of two water populations, in this permeable and disordered porous structure, has been discussed and confirmed using different formulation parameters: (i) different water-to-plaster ratios w/p (that mainly vary the total porosity); (ii) increasing additions of crushed gypsum (that mainly vary the total developed surface area). Thus, the continuous probing of the porous distribution of water and the measurements of the local mobility of proton populations have enabled a better knowledge of the evolving pore structure, without system perturbations. Progressive saturation and desaturation experiments were performed on samples of hardened gypsum and have enabled the identification of a fast diffusion regime, which was responsible for the enhancement of all the measured relaxation rates. A theoretical model enabled us to show that the exchange rate W between the two water populations was very slow, whereas their own relaxation with the surface was very fast. Two modes of confinement of water were identified as a function of water-to-plaster ratio ($0.4 \leq w/p \leq 0.6$ and $0.7 \leq w/p \leq 1$) and were interpreted by two modes of organization of porous structure, in agreement with earlier studies of self-diffusion of water in hardened gypsum.

Acknowledgment. We gratefully acknowledge the "Association Nationale de la Recherche Technique" (CIFRE fellowship) and the Research Center of LAFARGE for their financial support.

References and Notes

(1) Abragam, A. *The principles of nuclear magnetism*; Oxford University Press: 1961.
(2) Halperin, W. P.; Jehng, J.-Y.; Song, Y.-Q. *Magn. Reson. Imag.* **1994**, *12*, 169−173.
(3) Bhattacharja, S.; Moukwa, M.; D'Orazio, F.; Jehng, J. Y.; Halperin, W. P. *Adv. Cem. Based Mater.* **1993**, *1*, 67−76.
(4) Jehng, J. Y.; Sprague, D. T.; Halperin, W. P. *Magn. Reson. Imag.* **1996**, *14*, 785−791.
(5) Barberon, F.; Korb, J.-P.; Petit, D.; Morin, V.; Bermejo, E. *Phys. Rev. Lett.* **2003**, *90*, 116103.
(6) Valckenborg, R. M. E.; Pel, L.; Hazrati, K.; Kopinga, K.; Marchand, J. *Mater. Struct.* **2001**, *34*, 599−604.
(7) Nestle, N. *Cem. Concr. Res.* **2004**, *34*, 447−454.
(8) Filippov, A. V.; Khosina, E. V.; Khosin, V. G. *J. Mater. Sci.* **1996**, *31*, 1809−1814.
(9) Filippov, A. V.; Altykis, M. G.; Khaliullin, M. I.; Rachimov, R. Z.; Lantsov, V. M. *J. Mater. Sci.* **1996**, *31*, 4369−4374.
(10) Filippov, A. V.; Skirda, V. D. *Colloid J.* **2000**, *62* (6), 759−764.
(11) Le Chatelier, H. *C. R. Acad. Sci.* **1883**, *96* (11), 715.
(12) Chappuis, J. *Colloids Surf.* **1999**, *156*, 223−241.
(13) Slichter, C. P. *Principles of magnetic resonance*; Springer: Berlin, 1978.
(14) Brunauer, S.; Emmett, P.; Teller, E. *J. Am. Chem. Soc.* **1938**, *60*, 309.
(15) Ridge, M. J.; Beretka, J. *Rev. Pure Appl. Chem.* **1969**, *19*, 17.
(16) Brownstein, K. R.; Tarr, C. E. *Phys. Rev. A* **1979**, *19*, 2446−2453.
(17) Kleinberg, R. L.; Kenyon, W. E.; Mitra, P. P. *J. Magn. Reson., Ser. A* **1994**, *108*, 206−214.
(18) Godefroy, S.; Korb, J.-P.; Fleury, M.; Bryant, R. G. *Phys. Rev. E* **2000**, *64*, 021605.
(19) Bhattacharja, S.; D'Orazio, F.; Tarczon, J. C.; Halperin, W. P. *J. Am. Ceram. Soc.* **1989**, *72* (11), 2126−30.
(20) D'Orazio, F.; Bhattacharja, S.; Halperin, W. P. *Phys. Rev. B* **1990**, *42*, 16.
(21) Halperin, W. P.; Bhattacharja, S.; D'Orazio, F. *Magn. Reson. Imag.* **1991**, *9*, 733−737.
(22) Fripiat, J. J.; Letellier, M.; Levitz, P. *Philos. Trans. R. Soc. London, Ser. A* **1984**, *311*, 287−299.
(23) Levitz, P. E. *Adv. Colloid Interface Sci.* **1998**, *76*−*77*, 71−106.
(24) Plassais, A.; Pomies, M.-P.; Lequeux, N.; Korb, J.-P.; Petit, D.; Barberon, F.; Bresson, B. *Phys. Rev. E* **2005**, *72*, 041401−8.
(25) McDonald, P. M.; Korb, J.-P.; Mitchell, J.; Monteilhet, L. *Phys. Rev. E* **2005**, *72*, 011409−9.